2020 IEEE/RSJ International Conference on Intelligent Robots and Systems (IROS)
October 25-29, 2020, Las Vegas, NV, USA (Virtual)

2020 IEEE/RSJ International Conference on Intelligent Robots and Systems (IROS) | 978-1-7281-6212-6/20/$31.00 ©2020 IEEE | DOI: 10.1109/IROS45743.2020.9341442

Active Alignment Control-based LED Communication for Underwater Robots

Pratap Bhanu Solanki, Shaunak D. Bopardikar and Xiaobo Tan

***Abstract*— Achieving and maintaining line-of-sight (LOS) is challenging for underwater optical communication systems, especially when the underlying platforms are mobile. In this work, we propose and demonstrate an active alignment control-based LED-communication system that uses the DC value of the communication signal as feedback for LOS maintenance. Utilizing the uni-modal nature of the dependence of the light signal strength on local angles, we propose a novel triangular exploration algorithm, that does not require the knowledge of the underlying light intensity model, to maximize the signal strength that leads to achieving and maintaining LOS. The method maintains an equilateral triangle shape in the angle space for any three consecutive exploration points, while ensuring the consistency of exploration direction with the local gradient of signal strength. The effectiveness of the approach is first evaluated in simulation by comparison with extremum-seeking control, where the proposed approach shows a significant advantage in the convergence speed. The efficacy is further demonstrated experimentally, where an underwater robot is controlled by a joystick via LED communication.**

I. Introduction

LED-based underwater wireless optical communication is emerging as a promising, low-to-medium range alternative or complementary technology for acoustic communication, because of its attributes of low power consumption and high data rates [1], [2]. Many of the recent studies focused on increasing the range and data-rate of transmission. Examples include achieving a data rate of 4.8 gigabits per second (Gbps) over 5.4 m using a 450 nm laser diode [3], 7.2 Gbps for 6.8 m in seawater [4], and 15 Gbps for 20 m [5]. However, an inherent challenge associated with the optical communication systems is the requirement of the line-of-sight (LOS) between the communicating modules.

Several approaches have been proposed and implemented to address the issue of LOS. The use of multiple LEDs and/or photo-diodes has been reported [6], [7], [8], which eliminates the need for active alignment for the LOS. The redundancy in these systems leads to increased cost, power consumption, and system complexity. Modulating-retro-reflector (MRR)-based alignment systems have been developed for laser-based free-space optical communication (FSOC) systems [9], [10], [11], [12], where an MRR terminal is attached to a mobile platform, and most of the weight, power, and alignment mechanism requirements are placed on an active stationary ground station. This asymmetry makes the MRR-based systems unsuitable for mobile robot applications. Simulation studies on the use of 4 Quadrants Detectors (4QD) using step track and gradient ascent/descent algorithms [13], as well as Kalman filter [14], have been reported for optical beam tracking. Theoretical results supported by simulation studies have been presented by Bashir *et al.* [15] on the use of estimation techniques for a photo-detector array. These aforementioned systems also use redundancy at the receiver end, which is not desirable. A bi-directional free-space optical communication system that can auto-locate and align itself is demonstrated by Abadi *et al.* [16]; however, the system uses GPS and camera for redundancy in operation.

In this work, we propose and demonstrate an active alignment control-based LED-optical communication system for the underwater setting that uses a single LED (transmitter) and a single photo-diode (receiver). The signal from the photo-diode is used for both communication and feedback for alignment control. In our prior work [17], we have shown the tracking of an LED beam using an extended Kalman filter (EKF) in simulation and experiments in air. However, that approach assumes the knowledge of a precise light intensity model and hence requires significant effort in model identification. Furthermore, the approach relies on a constant *scanning* motion to ensure observability and thus convergence of the estimate. In this paper, we propose a novel triangular-exploration algorithm to achieve the maximum of light intensity, which corresponds to LOS with the transmitter.

The proposed algorithm moves the transceiver pointing direction in an equilateral triangular grid pattern and guarantees the pointing direction to be consistent with the local gradient direction. The method only requires the light intensity to be a unimodal function of the angle offsets from LOS, and does not require an explicit model for implementation. Furthermore, the approach also works directly for the setting of bi-directional communication. To benchmark the performance of our algorithm, we compare it with a perturbation based extremum-seeking control algorithm [18], [19], as it is also model-free and applicable to the bi-directional version of the alignment control problem. Simulation results show that the proposed triangular-exploration approach has more than one order of magnitude faster convergence to the point of maximum light intensity than the extremum-seeking algorithm. We further experimentally demonstrate the efficacy of the proposed triangular-exploration algorithm in simultaneous communication and tracking using an underwater robot. Considering the model-free and generic nature of our approach, it is applicable to a general scenario of local active alignment for single beam signals.

P.B. Solanki, S.D. Bopardikar and X. Tan are with the Department of Electrical and Computer Engineering, Michigan State University, East Lansing, MI, 48824 USA. Email: prabhanu@egr.msu.edu (P. B. S.), shaunak@egr.msu.edu (S.D.B.), xbtan@egr.msu.edu (X.T.).

Authorized licensed use limited to: Michigan State University. Downloaded on February 28,2021 at 05:35:55 UTC from IEEE Xplore. Restrictions apply.

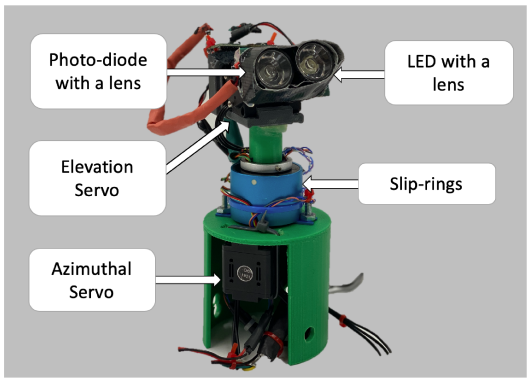

Fig. 1: Hardware description of the active transceiver module.

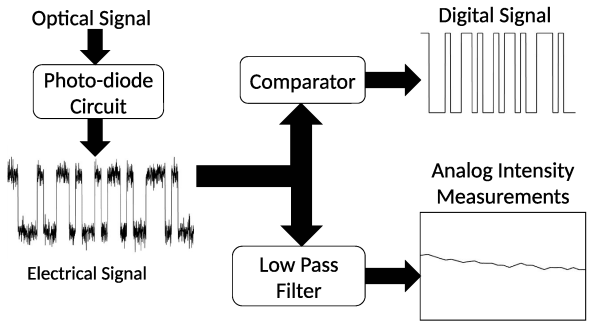

Fig. 2: Block Diagram illustrating the extraction of the signal strength and information from the received optical signal.

The organization of the rest of the paper is as follows. Section II discusses the basic problem set up. The details of the alignment algorithms are discussed in Section III. Simulation results are presented in Section IV, followed by the discussion on experimental setup and results in Section V. Finally, concluding remarks are provided in Section VI.

II. System Setup

Here, we first discuss the hardware setup and describe the relevant mathematical representation of the system behavior.

A. System Setup

Fig. 1 shows the hardware setup of the transceiver module. For the transmitter, a Cree XR-E Series LED with a principal wavelength of 480 nm is used, and for the receiver, a photo-diode from Advanced Photonix (part number PDB-V107). Two Dynamixel servo motors are used to control the azimuthal and elevation angles of the transceiver, respectively. Slip-rings are adopted to transmit the power and signals between the base stage and the rotation stage without the tangling of wires.

Fig. 2 illustrates the extraction of two components of the optical signal incident on the photo-diode. The optical signal is converted to an electrical signal by the photo-diode. The comparator converts the electrical signal to a digital signal based on a predefined threshold. The digital signal contains the *information* transmitted from the transmitter. When the electrical signal is passed through the low-pass filter, the DC component of the original signal is proportional to the intensity of the light received by the photo-diode and is used as feedback signal y for LOS search and maintenance in our work.

B. Received Light Intensity

As discussed in [17], the light intensity measurement y at the receiver, transmitted from a distance d, can be summarized as:

$$y = C_p I(\gamma) e^{-cd} g(\phi, \theta)/d^2, \tag{1}$$

where C_p is a constant of proportionality, γ is the angle between the transmitter's normal and the direction of LOS with the receiver. $I(\gamma)$ denotes the spatial intensity curve of the transmitter LED, which represents the intensity of light at unit distance and angle γ. The term c is the attenuation coefficient of the transmission medium (water in the current case). The terms ϕ and θ represent the azimuthal and elevation components of the angle of LOS with the receiver's normal in local coordinate system of the receiver. Fig. 3 illustrates the variables of interests and local coordinate systems. The coordinate frames are denoted as the *base-coordinate system* $(o - x'y'z')$ and the *receiver-coordinate system* $(o - xyz)$, respectively. Both coordinate systems share the same origin. The following sequential rule defines the axes of the frames:

- y' is the rotor's axis of base Dynamixel servo of the transceiver.
- x is the heading direction (normal) of the receiver.
- x' aligns with the zero angle of the base Dynamixel servo.
- z' is decided by the right hand rule.
- z and y are chosen such that z lies in $x' - z'$ plane, and the receiver-coordinate system aligns with the base-coordinate system when the heading direction (x-axis) aligns with the x'-axis.

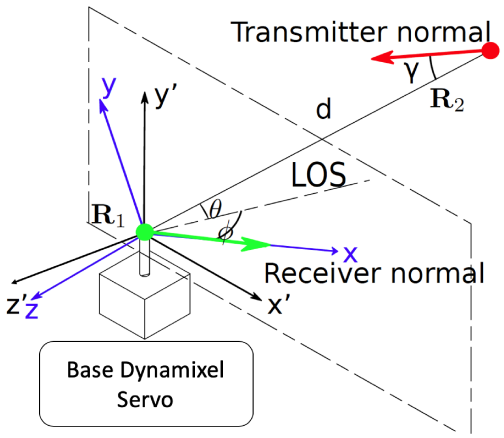

Fig. 3: Illustration of variables of interest and the relevant coordinate systems of the transceiver.

In the present work, we focus on local alignment control

Authorized licensed use limited to: Michigan State University. Downloaded on February 28,2021 at 05:35:55 UTC from IEEE Xplore. Restrictions apply.

techniques, and hence we consider a quasi-static light source, where it is assumed that the terms containing d and γ are constant or vary slowly as compared to ϕ and θ. The function g characterizes the receiver's field of reception and can be approximated by curve fitting of light intensity data collected for multiple values of ϕ and θ at constant d and γ, illustrated in Fig. 4. The figure shows that the function g is unimodal, which is the only requirement for the algorithms discussed in the next section.

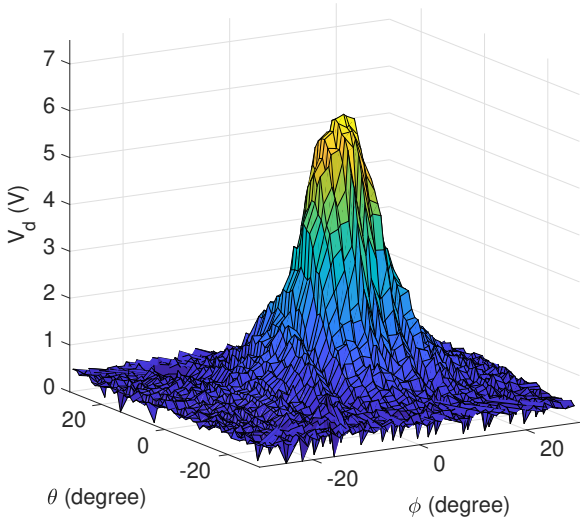

Fig. 4: Light intensity data for curve fitting of $g(\phi, \theta)$.

To facilitate the presentation, next we define the states of our system as the receiver's pointing direction as expressed in the base coordinate system, denoted by $\mathbf{x} = [x_1, x_2]^T$, where the system dynamics evolve in the discrete time as:

$$\begin{bmatrix} x_{1,k+1} \\ x_{2,k+1} \end{bmatrix} = \begin{bmatrix} x_{1,k} + u_{1,k} \\ x_{2,k} + u_{2,k} \end{bmatrix} \tag{2}$$

The unknown but fixed direction of LOS is denoted by $\mathbf{x}^* = [x_1^*, x_2^*]^T$, which can be approximated the by the following relation

$$\begin{bmatrix} x_1 - x_1^* \\ x_2 - x_2^* \end{bmatrix} \approx \begin{bmatrix} \phi \\ \theta \end{bmatrix}, \tag{3}$$

The approximation works well at low-elevation pointing direction of the receiver (state x_2) and is also used in modeling for simulation discussed in Section IV . The exact mathematical details are omitted for readability; however, it is implemented in the experiment. Henceforth, the output equation becomes

$$\mathbf{y}_k \approx C^{'} g(x_{1,k} - x_1^*, x_{2,k} - x_2^*), \tag{4}$$

with $C^{'}$ denoting a new constant which also captures γ and d. The desired control algorithm should steer the states $\mathbf{x}$ to a small neighborhood of $\mathbf{x}^*$ from any admissible initial value.

III. Alignment Control Algorithms

In this section, we first present the proposed alignment control algorithm and then briefly describe the implementation of the two-dimensional discrete-time extremum-seeking algorithm that is used for comparison in this work.

A. Triangular Exploration Algorithm

Given any initial condition $[x_{1,0}, x_{2,0}]^T$, we choose

$$\begin{bmatrix} u_{1,0} \\ u_{2,0} \end{bmatrix} = \begin{bmatrix} \delta\cos(\psi_0) \\ \delta\sin(\psi_0) \end{bmatrix}, \begin{bmatrix} u_{1,1} \\ u_{2,1} \end{bmatrix} = \begin{bmatrix} \delta\cos(\psi_0 + \Delta\psi_0) \\ \delta\sin(\psi_0 + \Delta\psi_0) \end{bmatrix}$$

where $\delta > 0$ is the step-size, with ψ_0 chosen randomly from $(-\pi, \pi]$ and $\Delta\psi_0 = \pm\frac{2\pi}{3}$, where the sign is chosen randomly. The above initialization places the first three values of the states $\mathbf{x}_0, \mathbf{x}_1$, and $\mathbf{x}_2$) in an equilateral triangle pattern. Now, define the control law $\mathbf{u}_k = [u_{1,k}, u_{2,k}]^T$ as follows:

$$\mathbf{u}_k = \begin{cases} \mathbf{x}_{k-1} - \mathbf{x}_{k-2}, & \text{if } \Delta\mathbf{y}_k \geq 0 \\ \mathbf{x}_{k-2} - \mathbf{x}_k, & \text{if } \Delta\mathbf{y}_k < 0, \end{cases} \tag{5}$$

where $\Delta\mathbf{y}_k = \frac{\mathbf{y}_k + \mathbf{y}_{k-1}}{2} - \mathbf{y}_{k-2}$. The control algorithm with the initialization ensures that the next, present and the previous states form vertices of on an equilateral triangle, as illustrated in Fig. 5. Consider three points, illustrated in Fig. 5 as, $\mathbf{x}_k$, $\mathbf{x}_{k-1}$ and $\mathbf{x}_{k-2}$ forming an equilateral triangle with side δ. There are only two possibilities for the next point $\mathbf{x}_{k+1}$; when $\Delta\mathbf{y}_k < 0$, the next point x_{k+1}^b comes back to the second previous point $\mathbf{x}_{k-2}$, and when $\Delta\mathbf{y}_k \geq 0$ the next point x_{k+1}^a completes the rhombus with the last three points. Further, the approximate gradient at point M_k (midpoint of segment joining $\mathbf{x}_{k-1}$ and $\mathbf{x}_k$) along the local coordinate axes $\hat{x}_k$ (direction of $\mathbf{x}_k - \mathbf{x}_{k-1}$) and $\hat{y}_k$ (direction orthogonal to $\hat{x}_k$), computed by finite difference is

$$\boldsymbol{\nabla}\mathbf{y}_k = \begin{bmatrix} \frac{\mathbf{y}_k - \mathbf{y}_{k-1}}{\delta} \\ \frac{\mathbf{y}_k + \mathbf{y}_{k-1} - 2\mathbf{y}_{k-2}}{\sqrt{3}\delta} \end{bmatrix}.$$

The second component of the gradient is a scalar multiple of $\Delta\mathbf{y}_k$, and the next point always lies on the local $\hat{y}_k$ axis, which is orthogonal to the previous direction of motion, in the increasing direction of the component of the gradient in $\hat{y}_k$.

B. Benchmark Approach: Extremum seeking (ES) Control

For comparison, we consider a two-variable version of the discrete-time extremum seeking control algorithm [19]. The block diagram in Fig. 6 illustrates the details of the implementation. The perturbation signals $A\sin(\omega_p k)$ and $A\cos(\omega_p k)$ are applied to each of the current mean of the states: $\hat{x}_{1,k}$ and $\hat{x}_{2,k}$, and then the perturbed states are put into the plant. The resulting plant output $\mathbf{y_k}$ is passed through a high-pass filter (HPF). The filtered output is multiplied by the corresponding perturbation signals to generate the biases $\xi_{1,k}$ and $\xi_{2,k}$, which are then used to update the mean of the states (through a discrete-time version of "integration") completing a feedback loop with the plant. The initial value

Authorized licensed use limited to: Michigan State University. Downloaded on February 28,2021 at 05:35:55 UTC from IEEE Xplore. Restrictions apply.

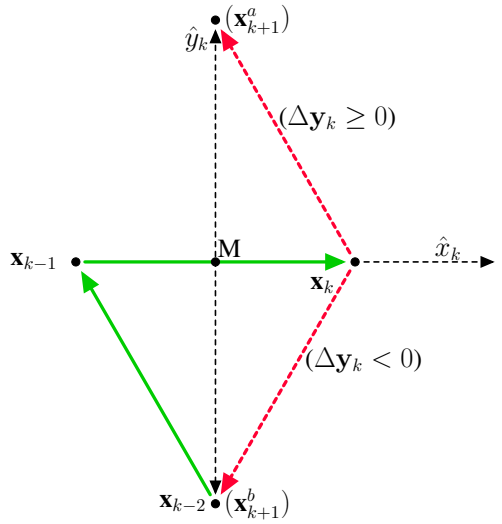

Fig. 5: Illustration of the triangular-exploration method.

of the mean of the states is chosen as the initial condition $[x_{1,0}, x_{2,0}]^T$.

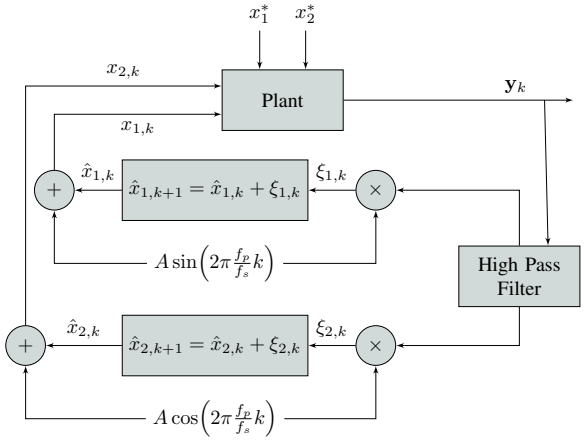

Fig. 6: Block Diagram for extremum seeking control.

IV. Simulation Results

In this section, we run simulation to study the performance of the two approaches to alignment control as described in the previous section. For generating the simulated intensity measurement y for the system, the measurement function $g(\phi, \theta)$ is taken to be a Gaussian function that is fitted to the data shown in Fig. 4:

$$g(\phi, \theta) = \exp\left(-\frac{\phi^2 + \theta^2}{a^2}\right) \tag{6}$$

with a characterizing the width of the reception of photo-diode. For a fair comparison between the triangular-exploration algorithm and the extremum-seeking (ES) algorithm, we choose the same sampling frequency f_s for each of them. Furthermore, the perturbation frequency f_p of the ES algorithm is chosen to be one-third of f_s so that the two-dimensional perturbation pattern of the ES algorithm becomes an equilateral triangle as well. Next, the size of the equilateral triangle of each of the algorithms is also made equal by choosing appropriate step-size δ and perturbation amplitude A respectively. Table I lists the values of all the parameters used in the simulation.

TABLE I: Parameters used in simulation.

Parameter	Value	Description
a	20°	Gaussian width for function g
f_s	100 Hz	Sampling frequency
f_p	33.33 Hz	Perturbation frequency
A	1°	Perturbation amplitude
K	500	Summation gain for extremum-seeking
r	$5\sqrt{3}^\circ$	Amplitude of circular motion for time varying optimum case
δ	$\sqrt{3}^\circ$	Step size for triangular-exploration algorithm

Fig. 7 shows trajectories of the states from the starting point **S**, under the proposed triangular exploration algorithm and the ES algorithm, respectively. It can be seen that, under each algorithm, the state converges to the neighborhood of the optimum point **O**. The triangular exploration algorithm moves in a zig-zag way but in a fixed direction for some time in the beginning. It then corrects itself frequently to follow the gradient and reach the neighborhood of the optimum point. The mean path of the ES algorithm follows the gradient and goes straight towards the optimum point. However, it is to be noted that while traversing the path, it spends a considerably large amount of time on exploration, and hence the actual speed of convergence is slower than the triangular exploration algorithm. It is important to note that both of the algorithms continue to oscillate around the optimum even after reaching a finite neighborhood around it. These oscillations are necessary in reality, especially when the optimum point is time-varying (for example, when the two communicating parties are moving with respect to each other), as we study next.

We consider a case when the optimum point has the following dependence on time:

$$\begin{bmatrix} x^*_{1,k} \\ x^*_{2,k} \end{bmatrix} = \begin{bmatrix} r\cos(2\pi f_M k/f_s) \\ r\cos(2\pi f_M k/f_s) \end{bmatrix} \tag{7}$$

which essentially means that the optimum circles the origin at the rate of f_M (frequency of *motion*) cycles per second at the radius of r degrees. Fig. 8 illustrates the evolution of states and the output for both of the algorithms for this time-varying optimum scenario. It can be observed that the states of the triangular exploration approach converge to the trajectory of optimum significantly faster than the states of ES approach. Further, there is a small lag in the tracking for the ES approach. The outputs of both of the approaches eventually converge close to the maximum value. which is 1 V.

Authorized licensed use limited to: Michigan State University. Downloaded on February 28,2021 at 05:35:55 UTC from IEEE Xplore. Restrictions apply.

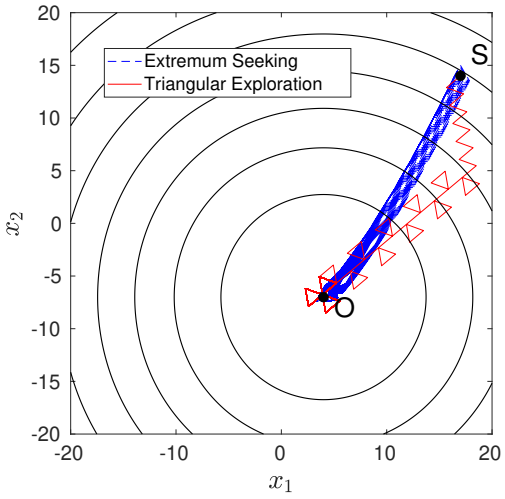

Fig. 7: Illustration of the paths traversed by extremum-seeking and triangular exploration algorithms.

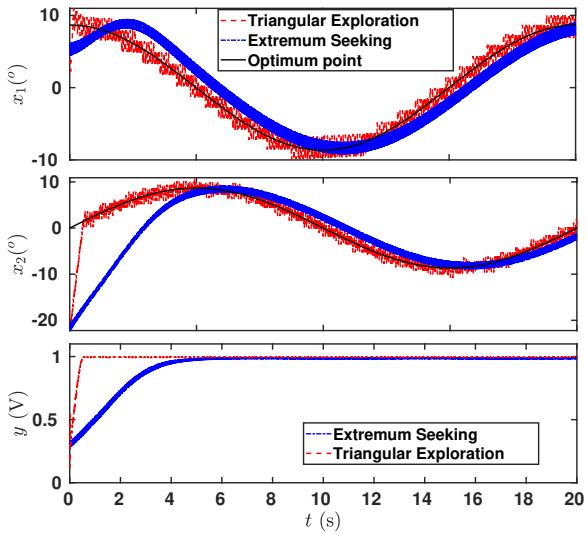

Fig. 8: Illustration of tracking of optimum points by the two algorithms, when the optimum is time-varying with $f_M = 0.05$ Hz.

To further characterize the performance and limitations of the algorithms when tracking a moving optimum, we simulate the algorithms over a range of speeds of motion; $f_M \in [0.001, 10]$ Hz. To illustrate the average tracking performance, we consider a metric called *mean steady-state error* e_m, which is defined as

$$e_m = \frac{1}{100} \sum_{k=n_f-99}^{n_f} \|\mathbf{x}_k - \mathbf{x}_k^*\|, \tag{8}$$

where n_f is the total number of iterations in one simulation run of an algorithm and $\|\cdot\|$ denotes the Euclidean norm of a vector. The number 100 is considered to effectively capture the average of steady-state points. Next, for each of the considered frequency of motion, we generate 1000

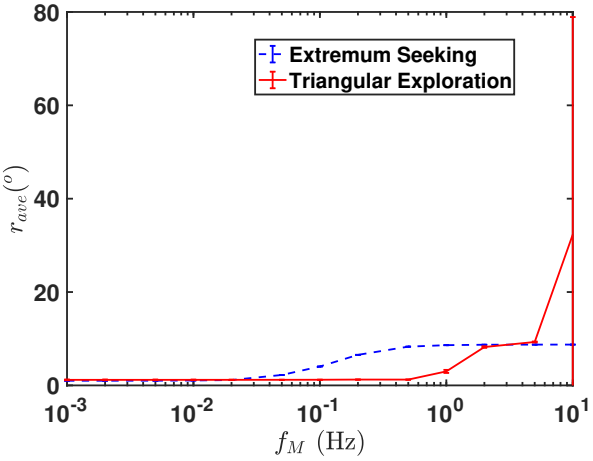

Fig. 9: Average mean steady-state errors in tracking a moving optimum over a range of f_M by each of the two algorithms.

initial points from the set ($\mathbf{x}_0 \in (-30^o, 30^o) \times (-30^o, 30^o)$) using the Latin Hypercube Sampling (LHS) technique in Matlab, and perform a simulation run for each of these initial conditions. The average and standard deviation of e_m from all of these runs yield the cumulative tracking performance at the particular frequency of motion. Fig. 9 shows the average tracking performance with the error bars over a range of speeds of motion. Fig. 9 suggests that *the triangular exploration algorithm can track the moving optimum by at least one order of magnitude faster as compared to the extremum-seeking approach*. Hence for the experimental work, presented next, we have only considered the triangular exploration algorithm. It is to be noted that ES algorithm shows a plateau as it converges to the center of the circle of motion however triangular algorithm shows high variation in the tracking performance as it does not show any convergence at high frequencies.

V. Experiment Setup and Results

In this section, we first describe our experimental setup, which comprises an underwater robot and an optical wireless joystick. Fig. 10 shows an underwater robot equipped with the transceiver module, described in Section II, inside a transparent casing. It consists of three T100 thrusters from Blue Robotics: two for horizontal motion and the other one for vertical motion of the robot. The robot is kept neutrally buoyant for ease of operation. For on-board processing and computation, a BeagleBone™ blue computer board is used.

Fig. 11 shows an optical communication-based joystick controller, where a PS4 joystick is integrated with the LED communication circuitry. The joystick is inspired by *diver interface module* [20], where high-level commands were transmitted by a human scuba diver to a robotic fish using acoustic communication. The joystick in this work is intended to direct the aforementioned robot in the underwater scenario by sending commands *"go up", "go forward", "turn left"*, etc. The commands corresponding to the buttons pressed on the joystick are received by an on-board BeagleBone™ blue

Authorized licensed use limited to: Michigan State University. Downloaded on February 28,2021 at 05:35:55 UTC from IEEE Xplore. Restrictions apply.

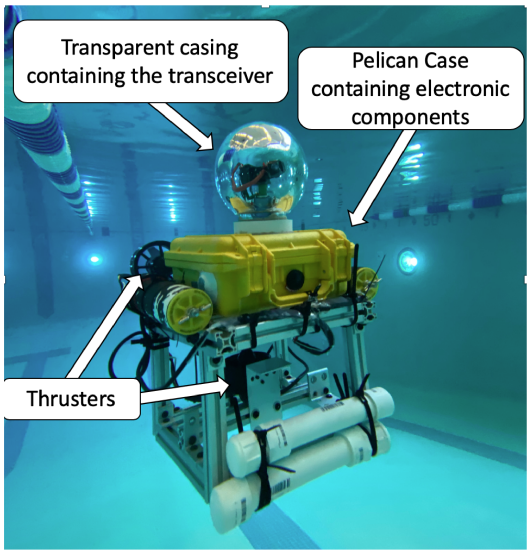

Fig. 10: An underwater robot equipped with the active transceiver.

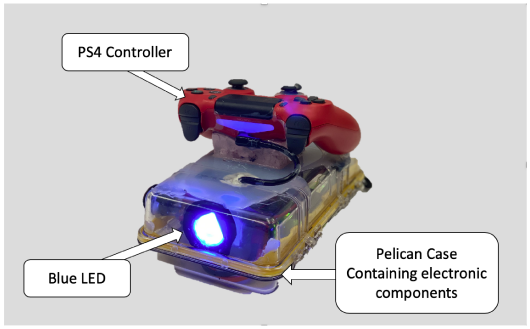

Fig. 11: A uni-directional LED-communication based joystick controller designed for this work.

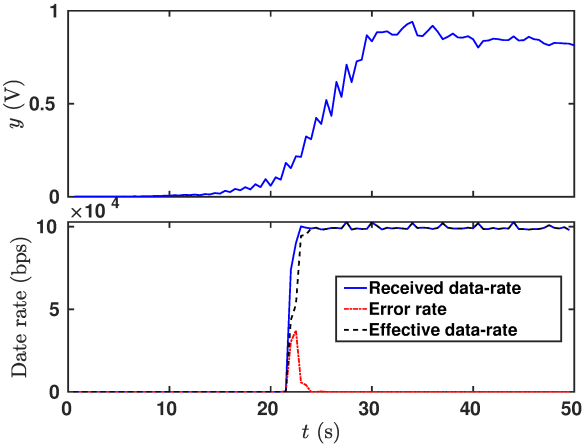

Fig. 12: Evolution of light intensity and data rates for an experiment run of triangular exploration algorithm on the experiment setup. The received data-rate is correlated with the signal-strength.

computer through a USB cable. The board then generates on-off keying (OOK) signals by the UART (Universal Asynchronous Receiver/Transmitter) protocol at a baud-rate of $115,200$ bits per second (bps), which are then transmitted through the LED of the joystick-controller. In addition, a predefined *dummy* string of characters is always transmitted repetitively from the LED to generate a constant average light intensity that facilitates active alignment control at the receiver end of the robot.

On the robot's end, the optical signals are received by the photo-diode and the two components, the average value y, and the information signal, are passed on to the on-board computer, which then uses the triangular exploration algorithm to steer the transceiver to align with the LOS. Fig. 12 shows the plots of the received signal intensity y along with bit-rates of reception and error rates over the course of an algorithm run. For this experiment, the robot is held steady underwater, and the LED-joystick is held about a meter away, pointing at the transceiver's location of the robot. The controller only transmits the dummy string, so that it is easier to compute the bit error rate on the other end. The received data-rate is computed by dividing the number of bits received by the length of the iteration interval (0.5 s). Since the expected incoming string is known, the bit-error-rate is computed by calculating the hamming distance between the received and expected bit strings.

At the beginning of the experiment, the transceiver of the robot was pointing away from the LED-joystick, and hence the received signal signal-strength was too low (less than the threshold of the comparator) for enabling communication. As time progresses, the signal strength increases, and at about the 21 second mark, the receiver starts receiving some bits. However, a major portion of the bits have error at this point. Here, the signal strength must be comparable to the comparator threshold resulting in a high signal to noise ratio (SNR). Moving forward, at about 25 seconds, as the signal strength increases further, the bit error eventually dissipates to zero, and the received information rate stabilizes to a value of about 10 Kbps, which is close to the baud-rate of transmission. The difference between the rates is attributed to the parity bit, which is used for built-in error correction by the UART protocol. At about 30 seconds, the signal strength gets saturated around a constant intensity; at this point, it is also visually observed that the transceiver pointing direction oscillates around the LOS with the LED-controller.

The setup is further tested in a swimming pool facility at the Michigan State University. The LED-controller is made operational underwater by sealing inside a transparent plastic bag so that the buttons remain accessible, and the light of LED is not blocked. Fig. 13 shows a human operator directing the robot to navigate inside the pool. The robot is commanded to move forward, backward, turn, and move upward/downward. It is to be noted that the human supervisor sometimes manually adjusts the pointing direction of the joystick to re-establish LOS with the robot's transceiver as the LOS gets disturbed due to fast relative motion between the robot and the controller.

VI. Conclusion and Future Work

In this work, we presented an active alignment control-based LED communication system for underwater robots.

Authorized licensed use limited to: Michigan State University. Downloaded on February 28,2021 at 05:35:55 UTC from IEEE Xplore. Restrictions apply.

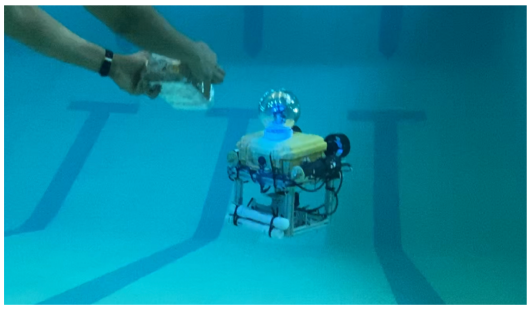

Fig. 13: Underwater robot being commanded by a human operator using the LED-joystick controller inside a swimming pool.

Given that the dependence of received light intensity on the local angles is unimodal, we proposed a triangular-exploration algorithm for real-time alignment control to achieve and maintain LOS. The algorithm ensures that the last three points always form an equilateral triangle so that it has a good estimate of the local gradient, and it uses the last three measurements to decide its next step in the gradient direction while maintaining the equilateral triangle shape. The tracking performance of the approach was compared with an extremum-seeking control method and was observed to have a significantly improved convergence rate. The efficacy of the algorithm was tested on an underwater experimental setup, where the dependence of data-rate on signal-strength was also demonstrated. Furthermore, the system was demonstrated for an application where a human operator wirelessly controlled a robot in an underwater scenario using an LED communication-based joystick.

Although the presented results are validated on the specialized hardware setup, the model-free and generic nature of the approach makes the results widely useful for scenarios of active alignment of single beam signals. For future work, we plan to create another copy of the underwater robot to demonstrate our approach in a bi-directional communication and collaboration setting. We will further perform comprehensive experiments to investigate and improve the robustness of our approach to challenging situations with noise and water disturbances.

ACKNOWLEDGMENTS

This work was supported by the National Science Foundation (IIS 1734272). The authors would like to thank John Thon, Austin Coha, and Shaswat Joshi for their help and support in developing the mechanical design of the underwater robot and performing the underwater experiments.

REFERENCES

[1] F. Hanson and S. Radic, "High bandwidth underwater optical communication," *Appl. Opt.*, vol. 47, no. 2, pp. 277–283, Jan 2008.

[2] C. Fei, X. Hong, G. Zhang, J. Du, Y. Gong, J. Evans, and S. He, "166 Gbps data rate for underwater wireless optical transmission with single laser diode achieved with discrete multi-tone and post nonlinear equalization," *Optics Express*, vol. 26, no. 26, 2018.

[3] H. M. Oubei, J. R. Duran, B. Janjua, H.-Y. Wang, C.-T. Tsai, Y.-C. Chi, T. K. Ng, H.-C. Kuo, J.-H. He, M.-S. Alouini, G.-R. Lin, and B. S. Ooi, "4.8 gbit/s 16-qam-ofdm transmission based on compact 450-nm laser for underwater wireless optical communication," *Opt. Express*, vol. 23, no. 18, pp. 23 302–23 309, Sep 2015.

[4] T. C. Wu, Y. C. Chi, H. Y. Wang, C. T. Tsai, and G. R. Lin, "Blue laser diode enables underwater communication at 12.4 gbps," *Scientific Reports*, vol. 7, no. January, pp. 1–10, 2017. [Online]. Available: http://dx.doi.org/10.1038/srep40480

[5] C. Shen, Y. Guo, H. M. Oubei, T. K. Ng, G. Liu, K.-H. Park, K.-T. Ho, M.-S. Alouini, and B. S. Ooi, "20-meter underwater wireless optical communication link with 15 Gbps data rate," *Optics Express*, vol. 24, no. 22, 2016.

[6] D. Anguita, D. Brizzolara, and G. Parodi, "Building an underwater wireless sensor network based on optical ommunication: Research challenges and current results," in *Sensor Technologies and Applications, 2009. SENSORCOMM'09. Third International Conference on*. IEEE, 2009, pp. 476–479.

[7] I. Rust and H. Asada, "A dual-use visible light approach to integrated communication and localization of underwater robots with application to non-destructive nuclear reactor inspection," *Robotics and Automation (ICRA), 2012 IEEE International Conference on*, pp. 2445–2450, May 2012.

[8] J. Simpson, B. Hughes, and J. Muth, "Smart transmitters and receivers for underwater free-space optical communication," *Selected Areas in Communications, IEEE Journal on*, vol. 30, no. 5, pp. 964–974, June 2012.

[9] P. G. Goetz, W. S. Rabinovich, R. Mahon, J. L. Murphy, M. S. Ferraro, M. R. Suite, W. R. Smith, B. B. Xu, H. R. Burris, C. I. Moore, W. W. Schultz, B. M. Mathieu, K. Hacker, S. Reese, W. T. Freeman, S. Frawley, and M. Colbert, "Modulating retro-reflector lasercom systems at the naval research laboratory," *Proceedings - IEEE Military Communications Conference MILCOM*, pp. 1601–1606, 2010.

[10] P. G. Goetz, W. S. Rabinovich, R. Mahon, M. Ferraro, J. L. Murphy, M. R. Suite, C. I. Moore, H. R. Burris, W. R. Smith, and W. W. Schultz, "Mobile lasercom systems using modulating retro-reflectors," in *Imaging and Applied Optics*. Optical Society of America, 2011, p. LWC2.

[11] W. S. Rabinovich, R. Mahon, P. G. Goetz, L. Swingen, J. Murphy, M. Ferraro, R. Burris, M. Suite, C. I. Moore, G. C. Gilbreath, and S. Binari, "45 Mbps cat's eye modulating retro-reflector link over 7 Km," in *Free-Space Laser Communications VI*, A. K. Majumdar and C. C. Davis, Eds., vol. 6304, International Society for Optics and Photonics. SPIE, 2006, pp. 172 – 182.

[12] B. Born, I. R. Hristovski, S. Geoffroy-Gagnon, and J. F. Holzman, "All-optical retro-modulation for free-space optical communication," *Opt. Express*, vol. 26, no. 4, pp. 5031–5042, Feb 2018.

[13] N. Nakarach and P. Cherntanomwong, "The comparison of optical beam tracking algorithm for free space optics," in *2017 International Electrical Engineering Congress (iEECON)*, March 2017, pp. 1–4.

[14] G. Soysal and M. Efe, "Kalman filter aided cooperative optical beam tracking," *Radioengineering*, vol. 19, p. 242, 06 2010.

[15] M. S. Bashir and M. R. Bell, "Optical beam position tracking in free-space optical communication systems," *IEEE Transactions on Aerospace and Electronic Systems*, vol. 54, no. 2, pp. 520–536, April 2018.

[16] M. M. Abadi, M. A. Cox, R. E. Alsaigh, S. Viola, A. Forbes, and M. P. J. Lavery, "A space division multiplexed free-space-optical communication system that can auto-locate and fully self align with a remote transceiver," *Scientific Reports*, vol. 9, no. 1, p. 19687, 2019. [Online]. Available: https://doi.org/10.1038/s41598-019-55670-1

[17] P. B. Solanki and X. Tan, "Extended Kalman filter-based 3D active-alignment control for LED communication," in *2018 IEEE International Conference on Robotics and Automation, ICRA 2018, Brisbane, Australia, May 21-25, 2018*, 2018, pp. 4881–4888. [Online]. Available: https://doi.org/10.1109/ICRA.2018.8460949

[18] Joon-Young Choi, M. Krstic, K. B. Ariyur, and J. S. Lee, "Extremum seeking control for discrete-time systems," *IEEE Transactions on Automatic Control*, vol. 47, no. 2, pp. 318–323, Feb 2002.

[19] M. Krstic and K. B. Ariyur, *Multiparameter Extremum Seeking*. John Wiley Sons, Ltd, 2004, ch. 2, pp. 21–45.

[20] R. K. Katzschmann, J. DelPreto, R. MacCurdy, and D. Rus, "Exploration of underwater life with an acoustically controlled soft robotic fish," *Science Robotics*, vol. 3, no. 16, 2018.

Authorized licensed use limited to: Michigan State University. Downloaded on February 28,2021 at 05:35:55 UTC from IEEE Xplore. Restrictions apply.